

Experimental and Numerical Study for Turbulent Flow Drag Reduction in District Cooling Systems

Mohamed M. Abo El-Azm¹, Sadek Z. Kassab², Sameh A. Elshafie^{1C}

¹*Mechanical Engineering Department, College of Engineering and Technology, Arab Academy for Science and Technology, Alexandria, EGYPT*

²*Mechanical Engineering Department, Alexandria University, Alexandria, EGYPT*

Received: 11/03/2014 – Revised 10/06/2014 – Accepted 13/07/2014

Abstract

In the present study an experimental and numerical investigations were performed for District Cooling system in order to optimize the energy consumption as an application of the drag reduction phenomena. Simulation was carried out using finite volume method In order to maximize system efficiency by reducing pumping power due to the appearance of drag reduction phenomenon at certain concentrations of ethylene glycol in water. The drag reducing agent that was used is ethylene glycol (C₂H₆O₂) which is considered as an organic liquid compound to be used as anti-freeze. Several concentrations were tested and the simulation results were in fair agreement with the experimental cases studied. Results showed that with increasing ethylene glycol concentration the drag reduction increases till it reaches a maximum value of 10% at concentration of 4000 PPM and drops after that according to the drag reduction phenomena.

Keywords: CFD; turbulent; ethylene glycol; Drag reduction; correlation.

1. Introduction

In terms of ENERGY and SAVINGS District Cooling can reduce electricity usage by more than 65% compared to traditional air conditioning systems. As a comparison traditional chiller plants account for up to 70% of an organic compound the electricity usage in a large building. Thereby the individual power consumption is reduced substantially by a shift of load from each building to a central plant. And there will also be a substantial reduction of costs for operation and maintenance and costs for spare parts will be totally eliminated [1].

In terms of environmental benefits District Cooling also has a lot to offer, It is comfort and convenient for customers as there is no noisy equipment in the window or on the roof also improves energy efficiency and enhances environmental protections .Another main advantage is that it decrease building capital costs and improve architectural design flexibility.

Cornell University's Lake Source Cooling System uses Cayuga Lake as a heat sink to operate the central chilled water system for its campus and to also provide cooling to the Ithaca City School District. The system has operated since the summer of 2000 and was built at a cost of \$55–60 million. It cools a 14,500 tonsload.

^C Corresponding Author: Sameh A. Elshafie
Email: E-mail: sameh_elshafie@hotmail.com
© 2014 All rights reserved. ISSR Journals

It is well-known that the addition of a minute amount of polymer to a turbulent Newtonian fluid flow can result in a large reduction of the frictional drag in pipes and channels. Although this effect has been known for almost half a century, the physical mechanism that causes this drag reduction has still not been clearly identified. [2]

In pipe flows, for example, the drag can be reduced by up to 80 % by adding just a few parts per million (PPM) of polymer. This phenomenon leads to the possibility of increased capacities and faster shipping in pipelines. The discovery of this phenomenon of turbulent drag reduction by polymer additives is generally ascribed to Toms's [3].

Since Toms's discovery, the phenomenon has been studied widely, both experimentally and theoretically. Drag reduction here will be defined as any modification to a turbulent fluid flow system that results in a decrease in the normal rate of frictional energy loss and that leaves the resulting flow turbulent. Toms obtained friction reduction up to 50% compared with a pure solvent using a 0.25% solution of poly (methyl-methacrylate) in mono-chloro-benzene. He used tubes of various diameters and observed that:

Drag reduction occurs in turbulent flow and for a given polymer concentration and Reynolds number, it increases as the pipe diameter is reduced and also The drag reduction occurs when the wall shear stress exceeds a critical value which later came to be known as "onset of drag reduction". [3].

Since then, there has been number of attempts on drag reducing polymers for possible applications in fire extinguishing operations, crude oil transport, oil well operation, sewers and slurry transport. The positive results obtained in drag reducing phenomenon in above fields of technology have led the research work to try its possible application in district cooling system.

Yoon et al. investigated the effect of polymer additives in district heating and cooling system to produce obvious reductions in drag and heat transfer reduction are having observed. They found that comparing with well-known poly-crylamide ,copolymer additives are more effective and reliable in obtaining maximum drag reduction, and there also exist perfect conditions for mixing ratio of polymers, and with surfactants [4]. Kawaguchi et al. ,revealed that 70% of the pumping power used to drive hot water in primary pipelines or district heating systems was saved by adding only a few hundred PPM of surfactant into the circulating water. They introduce experimental and numerical studies on the turbulence structure in drag reducing flow. The result of an application study relating to the air conditioning system have been shown. [5]

In a review of the literature, the mechanism of additive-induced drag-reduction has not been clearly described. For polymer solutions, two theoretical explanations are given. One was proposed by Lumley, J.I. [6, 7], who postulated that the increased extensional viscosity due to the stretching of randomly coiled polymers tends to dampen the small eddies in the buffer layer and thickens the buffer layer, to give rise to the drag-reduction. Lumley emphasized that drag-reduction occurs only when the relaxation time of the solution is larger than the characteristic time scale of the turbulent flow.

In district cooling system, however, large pumping power is required because water has to travel long distances. If the pumping power can be reduced significantly using this drag reduction phenomenon, great energy saving in the system can be obtained and consequently the cooling system will become more feasible technically and economically. [4]

Xueming and Jianzhong (2002), studied the mechanism of drag reduction by polymer additives, the turbulent intensities and Reynolds stresses in a mixing layer and pipe flow are measured by LDA (Linear discriminate analysis) respectively. They concluded that polymer additives do not simply suppress the turbulent fluctuation. However the turbulence structures are changed rather than suppressed.

Al-Sarkhi (2010). Described the characteristics of the two-phase flow with drag reducing additives and introduced the research approaches and methodology concerning drag reduction with additives in multiphase flow. It's suggested that the mechanisms for drag reduction phenomena and procedure in two-phase flow are discussed. He explained some of the industrial application of the

use of drag reducing additives in two-phase flow. Finally, he highlighted recommendations, new suggested approaches for future research needs and potential areas that need further research.

The aim of the present work, therefore, is to carry out experimental and numerical investigations to study the effectiveness of ethylene glycol as a drag reducing agent; especially that it is already used as antifreeze in district cooling systems.

2. Experimental Setup

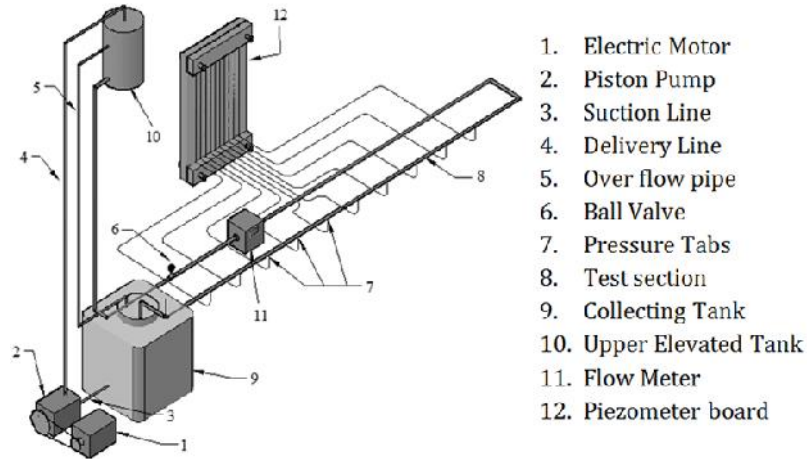


Figure 1: Experimental Setup layout

The experimental setup, shown in Figs.1, consists of a 1000 liters collecting tank, 500 liters constant-head upper elevated tank, a reciprocating piston pump (driven by D.C constant speed motor, ball valve, flow meter, and test section. The test section has ten pressure taps.

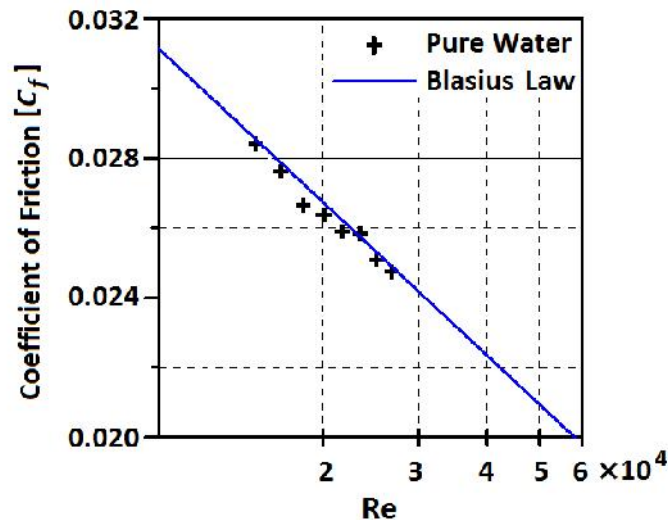


Figure 2: Comparison of the experimental coefficient of friction of pure water (zero PPM) with Blasius friction law at different Reynolds numbers

For the present study, tests were made on the test rig to prove that it's calibrated as shown in Fig. 2 the coefficient of friction of pure water in test rig was very close to Blasius equation, also the linearity of the wall static pressure drop was checked at the beginning using water only (zero concentration). A sample of results is shown in Fig. 3 for the range of Reynolds numbers, Re , ($1.5 \times 10^4 - 2.7 \times 10^4$). From this figure, it is clear that for all Reynolds numbers the static pressure drop along the pipe wall is linear and consequently the flow is fully developed.

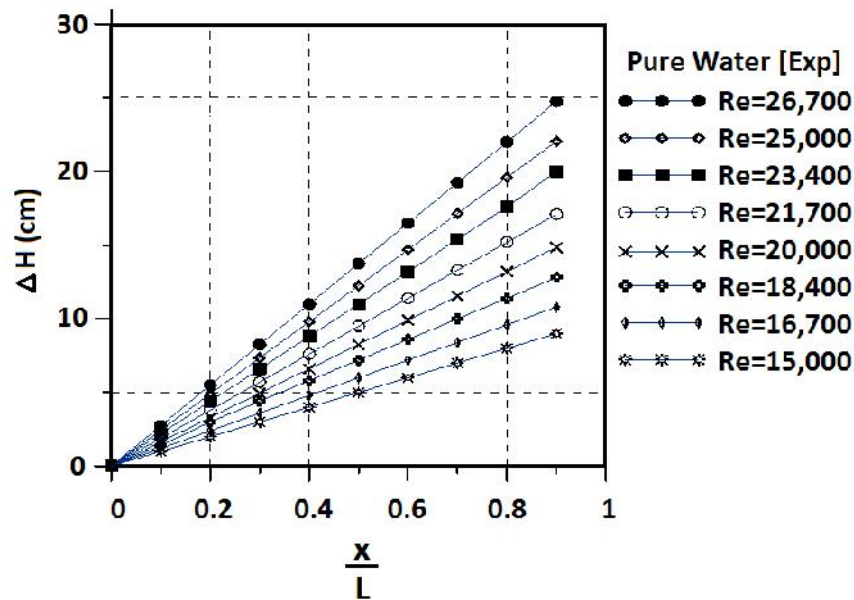


Figure 3: Static Pressure distributions along the test section of pure water at different Reynolds numbers

3. Numerical procedure

The present work was performed by means of a numerical method using a CFD (ANSYS fluent version 14) code. The method solves the three-dimensional, steady, incompressible Reynolds-averaged Navier–Stokes equations. The Reynolds stress is related to the mean velocity gradients by employing the Boussinesq approach, while the turbulence model adopts the Standard $k-\epsilon$ model. The basic governing equations are solved in the absolute frame and discretized by the finite volume technique. The discretization schemes used in this calculation are as follows: body force weighted scheme for pressure; simple algorithm for pressure–velocity coupling; and first-order accurate upwind scheme for momentum, turbulence kinetic energy (k) and turbulence dissipation rate (ϵ).

The geometry constructed to match the test loop in the experimental case study of selim, M.M., [8] for comparison purposes. Figure (4) shows isometric view of the geometry.

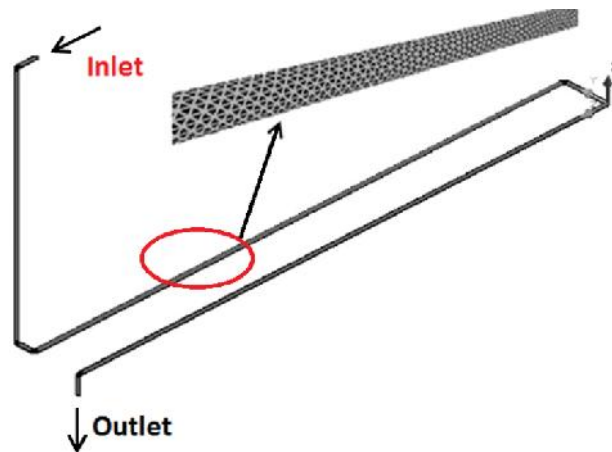


Figure 4: Mesh Generation (Tetra-Hydral) and Boundary conditions.

Figure 4 illustrates the mesh employed on the computational domain, which consists of triangular face mesh of size 4.8×10^{-6} and tetrahedral volume grids of size 2.98×10^{-3} . The total number of cells was 90272. The calculations on each case of solution concentration are carried out

steady flow condition for various values of Reynolds numbers, which is defined as the ratio of the inertia force to the viscous force.

$$Re = \frac{\rho v D}{\mu} = \frac{v D}{\nu} \quad (1)$$

In order to model a given situation and obtain a solution of the steady turbulent flow within the computational region, boundary conditions must be provided to supply the conservation equations as shown in Figure. . These include inlets, outlets and walls. The k- model requires some quantification of k and parameters at the inlets. It is possible to specify k and directly or indirectly by calculating the values from the inputs for turbulence intensity and the characteristic length. Versteeg and Malalasekera[15] give the following approximations:

$$k = \frac{3}{2} [U_{ref} T_i]^2 \quad (2)$$

$$\varepsilon = C_{\mu}^{3/4} \frac{k^{3/2}}{l} \quad (3)$$

$$l = 0.07 L \quad (4)$$

where T_i is the turbulence intensity which has the value of 0.75 and L is the characteristic length. In this study, the various values of Reynolds numbers were achieved by varying the inlet velocity of the solution. For the solution initialization, the calculations are performed under the relative to cell zone reference frame and the gauge pressure is set to zero. The convergence of solution is monitored by checking the residuals of the numerically solved governing equations. Moreover, in order to judge the convergence, the behaviour of other quantities, such as the total pressure at the inlet and outlet boundaries is also monitored.

Modelling turbulence flow requires appropriate modelling procedures to describe the effects of turbulent fluctuations of scalar quantities and velocities on the basic conservation equations. The conservation equation utilized for turbulent flows are obtained from the laminar form of the equations using a time averaging procedure called Reynolds averaging. By applying the Reynolds averaging to the scalar quantities in the governing equations, these can be resolved into their mean and fluctuating components. The models used are the standard k- model, standard k- model and the low Reynolds Launder-Sharma model.

3.1 The standard k- model

The standard k- model is a semi-empirical model based on model transport equations for the turbulent kinetic energy (k) and its dissipation rate (ε). The model transport equation for (k) is derived from the exact equation, while the model transport equation for (ε) is obtained using physical reasoning and bears little resemblance to its mathematically exact counterpart.

In the derivation of the k- model, it is assumed that the flow is fully turbulent, and the effects of the molecular viscosity are negligible. The standard k- model is therefore valid only for fully turbulent flow.

The turbulent kinetic energy (k) and its rate of dissipation (ε) are obtained from the flowing transport equations.

$$\rho \frac{dk}{dt} = \frac{\partial}{\partial x_i} \left[\left(\mu + \frac{\mu_t}{\sigma_k} \right) \frac{\partial k}{\partial x_i} \right] + G_k + G_b - \rho \varepsilon - Y_M \quad (5)$$

and

$$\rho \frac{d\varepsilon}{dt} = \frac{\partial}{\partial x_i} \left[\left(\mu + \frac{\mu_t}{\sigma_\varepsilon} \right) \frac{\partial \varepsilon}{\partial x_i} \right] + C_{1\varepsilon} \frac{\varepsilon}{k} (G_k + C_{3\varepsilon} G_b) + C_{2\varepsilon} \rho \frac{\varepsilon^2}{k} \quad (6)$$

In these equations, G_k represents the generation of turbulent kinetic energy due the mean velocity gradients. G_b is the generation of turbulent kinetic energy due to buoyancy. Y_M represents the contribution of the fluctuating dilatation in compressible turbulence to the overall dissipation rate. C_1 , C_2 and C_3 are constants. k and ε are the turbulent Prandtl numbers for k and ε , respectively.

The eddy or turbulence viscosity, μ_t , is computed by combining k and ε as follows,

$$\mu_t = \rho C_\mu \frac{k^2}{\varepsilon} \quad (7)$$

Where C_μ is a constant and the other model constants C_1 , C_2 , C_μ , k and ε have the following default values $C_1 = 1.44$, $C_2 = 1.92$, $C_\mu = 0.09$, $k = 1.0$ and $\varepsilon = 1.3$

These default values have been determined from experiments with air and water for fundamental turbulent shear flows including homogeneous shear flows and decaying isotropic grid turbulence. They have been found to work fairly well for a wide range of wall-bounded and shear flows, Rodi, W. and Mansour, N.N. [9]

- The convergence criterion for the continuity equation and the velocity components is 10-6, the k-epsilon is 10-4.
- The pressure-velocity coupling is simple,
- Types of linear equation solver (flow, volume fraction, slip velocity, turbulence),
- The under-relaxation factors are:

Pressure (0.3), density (1), body forces (1), momentum (0.7), slip velocity (0.1), volume fraction (0.2), turbulent kinetic energy (0.8), turbulent dissipation rate (0.8), turbulent velocity (1).

- The discretization:

-Pressure (body force weighted).

-Volume fraction is first order upwind.

-Momentum, turbulent kinetic energy and turbulent dissipation rate all are second order upwind.

3.2 Mesh dependency test:

All simulations were performed with three different meshes for all cases in order to check the mesh independence of the solution. Structured grid was used of different sizes as shown in (table1). Figure 5 shows the pressure distribution for three different meshes where the maximum error does not exceed 0.2% for all cases.

TABLE (1): DETAILS OF THE THREE GRIDS USED IN THE GRID INDEPENDENCY STUDY.

Grid No.	Number of cells	Minimum area (m ²)	Maximum area (m ²)	Total Volume	Nodes	Faces
M-1	90,272	4.84×10 ⁻⁶	5.27×10 ⁻⁵	2.98×10 ⁻³	21,228	191,687
M-2	104,345	3.66×10 ⁻⁶	4.26×10 ⁻⁵	2.46×10 ⁻³	26,175	224,353
M-3	175,589	2.71×10 ⁻⁶	3.96×10 ⁻⁵	2.485×10 ⁻³	42,968	376,068

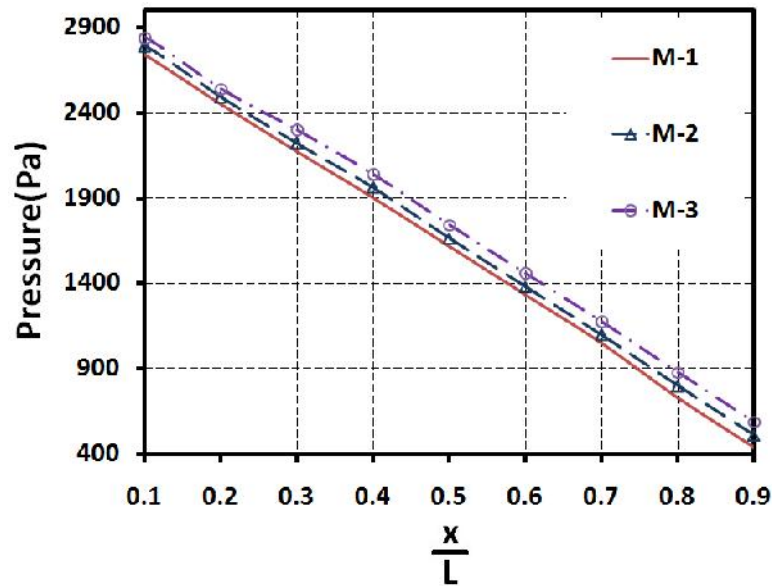


Figure 5: Static pressure distribution for Grid-dependence study

3.3 Numerical Results Validation

Figure 6 shows the pressure head loss for pure water run using $k-\epsilon$ model. For comparison purposes the experimental results was also included. As shown in this figure the two sets have the same trend, it was also found that there was a slight difference of (1cm) head-loss in magnitude between the experimental and simulation results.

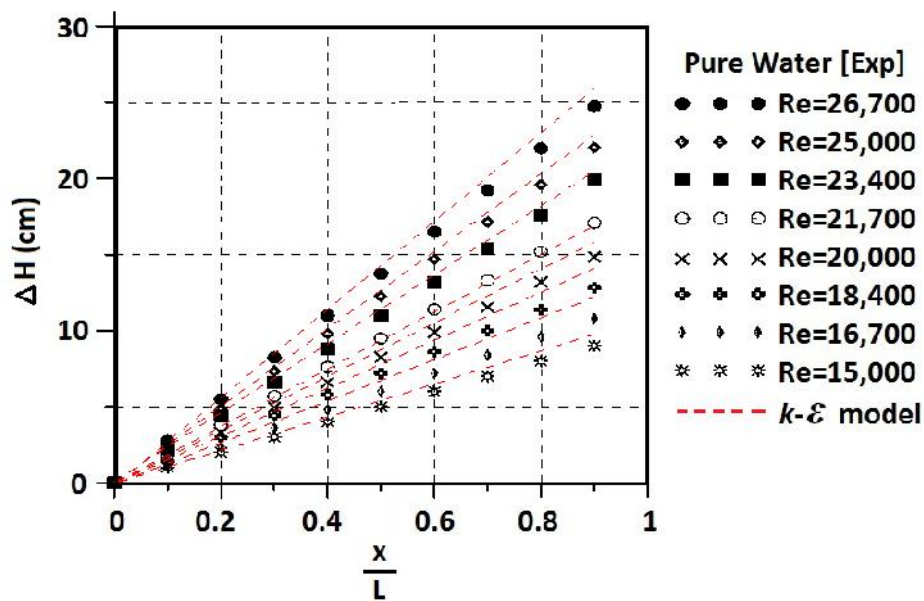


Figure 6: Experimental and numerical results for pressure distributions of pure water (zero PPM) at different Reynolds Numbers

4. Results and Discussion

Using $k-\epsilon$ model as a solver provides the closest simulation results to the experimental results. Consequently, it was used as the primary solver in the solving procedure, and all the numerical results presented in the following sections are obtained using $k-\epsilon$ model.

The minimum Reynolds number required to ensure fully turbulent flow was investigated thoroughly for the case of pipe and channel flows by [10]. There three criteria, namely, skin

friction-Reynolds number relation, log law with universal constants, and disappearance of intermittency, did not lead to unique minimum value of Reynolds number above which fully turbulent flow can be established. In the present study the minimum Reynolds number was 15000, i.e. the present pipe flow satisfies this requirements. [11].

First, static pressure distribution of pure water was monitored at various Reynolds numbers along the constructed model. The Reynolds numbers adjusted in the calculations to make it almost the same as those in the experimental case study. For pure water, zero PPM, Figure.7 shows that the resulted pressure distribution decreases gradually till it reaches the atmospheric pressure at the outlet port.

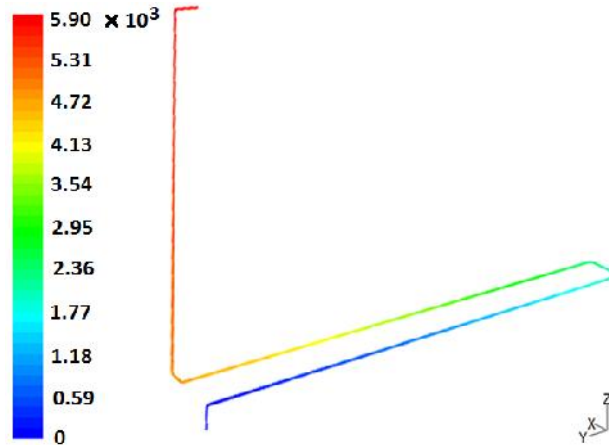


Figure 7: Static Pressure distribution (Pa) of pure water along the model at $Re_{avg}=26,700$

After apply the solving procedure for several concentrations the pressure distribution is monitored. Figure (8) shows a pressure distribution comparison between several ethylene concentrations at $Re=26,700$.

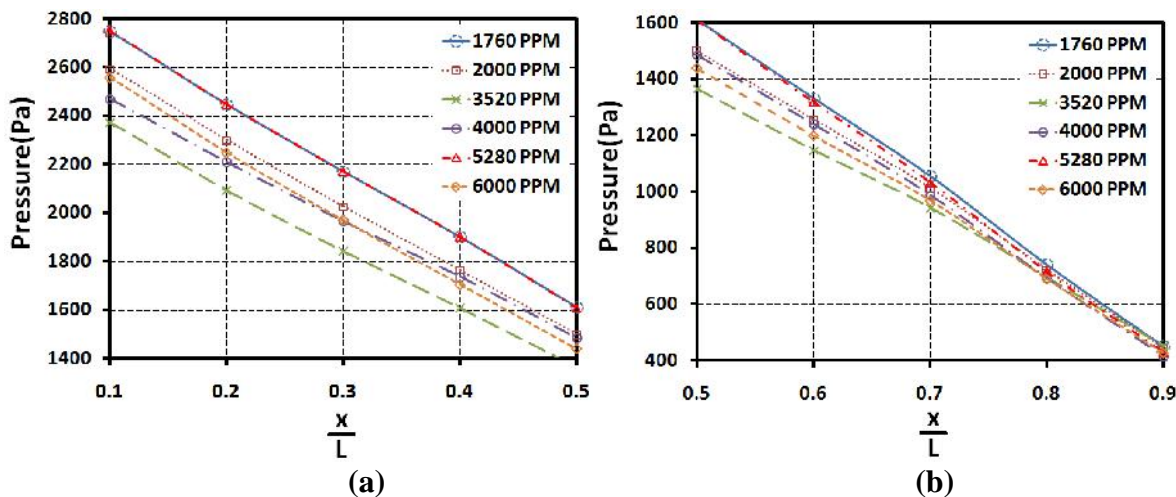


Figure 8: Static pressure distribution for different concentrations at $Re_{avg}=26700$, (a) $x/L=0$ to 0.5 and (b) $x/L=0.5$ to 0.9

By extracting the pressure values at each point on the model and applying Darcy's equation, coefficient of friction is obtained. Figure 9 shows the coefficient of friction for 4000 PPM solution (minimum head loss case) versus Reynolds number and compared with coefficient of friction obtained using Blasius friction law for pure water (zero PPM) concentration this law is considered the best law representing the friction of water through smooth pipes within the range of Reynolds numbers in the present study

$$C_f = 0.316 Re^{-0.25} \tag{8}$$

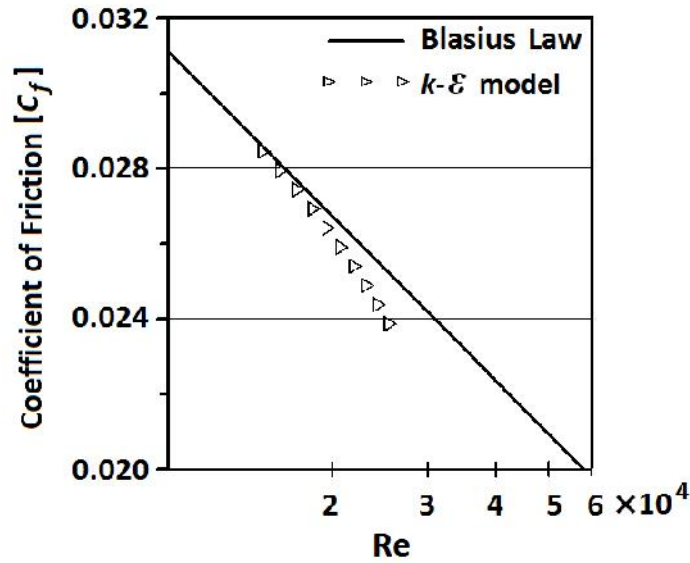


Figure 9: Coefficients of friction versus Reynolds number for 4000 PPM solution

Using Eq.20 drag reduction percentage is obtained at various concentrations for different Reynolds numbers. Figure 10 shows the drag reduction percentage at average Reynolds number of 26700. This figure is clearly shows that drag reduction percentage increases with concentration increases, after reaching maximum value of 10% approximately at 4000 PPM the percentage decreases again. As found by Gampert and Rensch[12], the DR% could be estimated from:

$$DR\% = \frac{C_{f_w} - C_{f_m}}{C_{f_w}} \times 100 \tag{9}$$

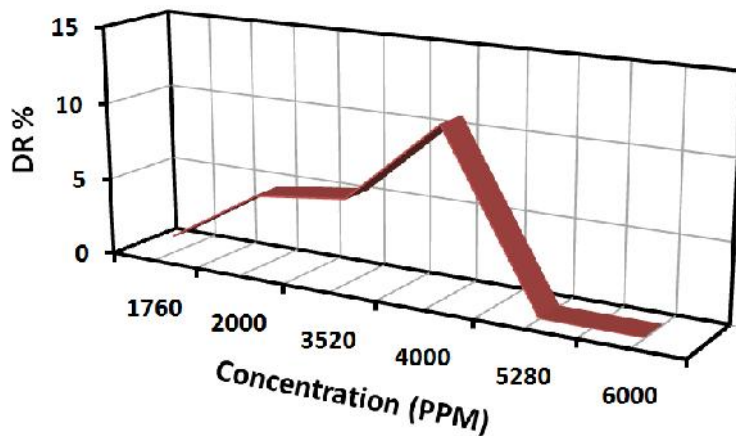


Figure 10: Percentage drag reduction when Re_{avg}=26700

Figure 10 describes the percentage drag reduction DR%, variation with ethylene glycol concentrations for experimental results. It's clear that the DR% increase with the increase of the concentration till it reaches the maximum DR% at concentration 4000PPM till it reaches about 10% then it starts to decrease again.

Figure 11 shows head loss versus distance ratio at different Reynolds numbers and different concentrations for both experimental and simulation results. Both results have the same trend that the percentage drag reduction increases with the increases of concentration till it reaches its

maximum value approximately at 4000 PPM and drops again after that concentration. For all concentrations, the simulation predicts higher values of percentage drag reduction compared with the corresponding experimental percentage drag reduction value. For all Reynolds numbers the simulated pressure head loss is greater than the experimental head loss.

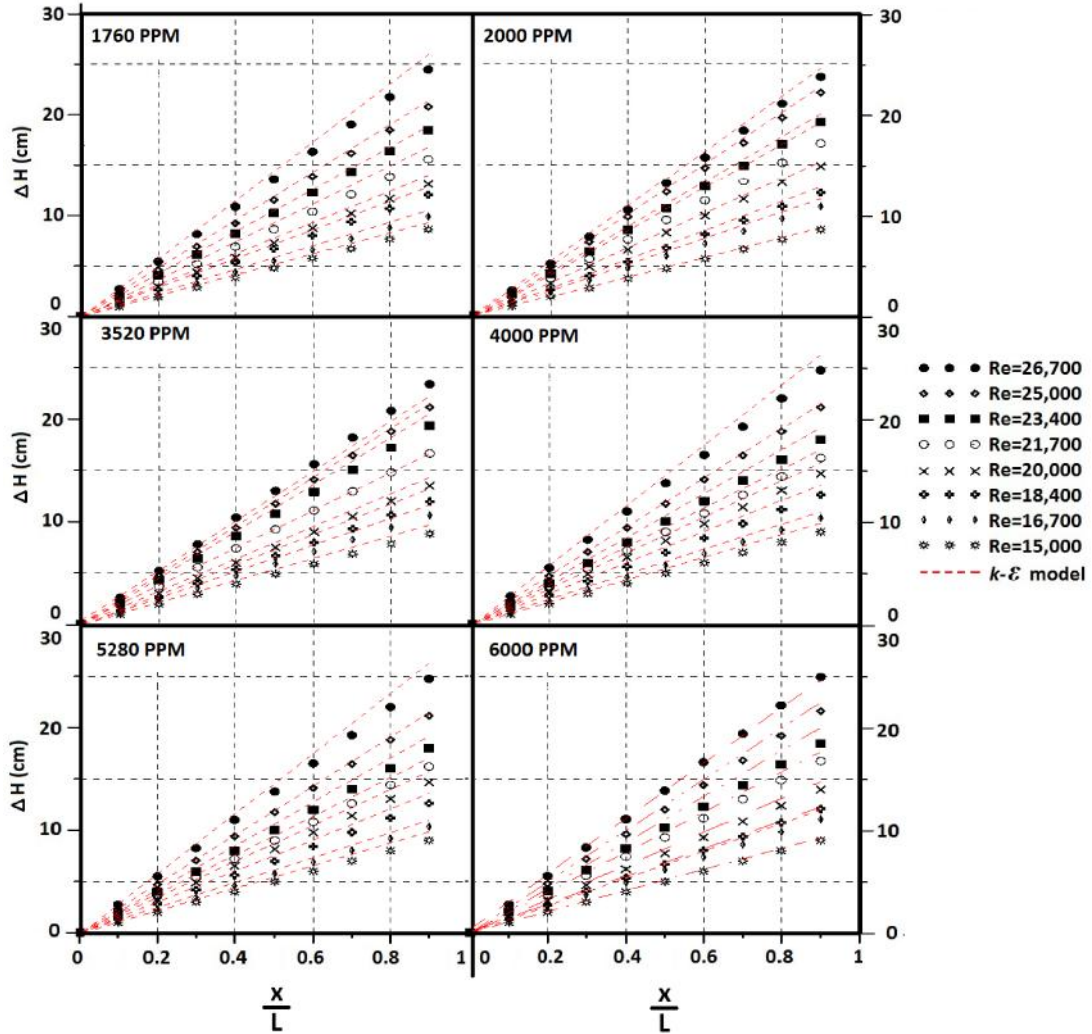


Figure 11: Experimental and simulation head loss (ΔH) versus distance ratio (x/L) at different Reynolds numbers (Re) and different concentrations in (PPM)

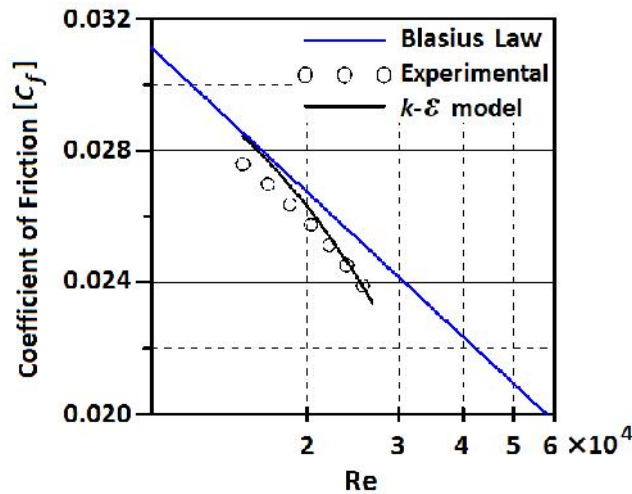


Figure 12: Coefficient of friction for experimental and simulation results compared with Blasius friction law for 4000 PPM

In order to compare the coefficient of friction in the experimental and numerical results Figure 12 is presented for the case of 4000 PPM. It is clear that the coefficient of friction obtained using simulation results have a lower curvature than that the one obtained using experimental measurements.

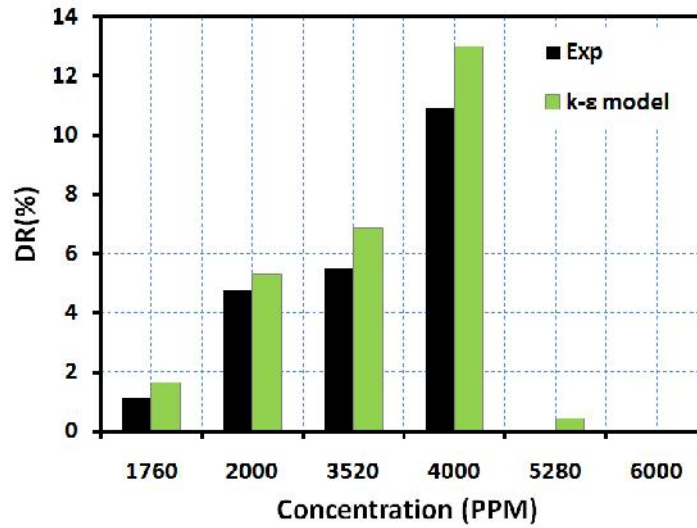


Figure 13: Percentage drag reduction(experimental and numerical) at different concentrations

The difference between the experimental and numerical results, shown in Figures 11 and 13, is coming from both techniques (experimental and numerical). The uncertainty in the experimental results is one input to this difference. In addition, the simplified assumptions in the used numerical technique are the other input. These two inputs can be in certain cases in the same direction and in other cases in the opposite direction. One thing should be mentioned here that a trial was performed to minimized this difference by choosing from the beginning the most suitable turbulence model closest to the experimental results, i.e. k- model.

4.2 Empirical correlations

Depending on the experimental results, equations for coefficient of friction at different concentration and different Reynolds numbers were estimated.

$$C_f = n \times Re^m \tag{10}$$

TABLE (2): CONSTANTS M AND N TO BE USED IN EQUATION (10)

CONCENTRATION	N	M	MAXIMUM ERROR
1760	0.28	-0.244	0.16%
2000	0.109	-0.146	0.12%
3520	0.444	-0.288	0.16%
4000	0.909	-0.374	0.14%
5280	0.663	-0.327	0.11%
6000	0.574	-0.312	0.12%

Table 2 presents the (m, n) the constants depending on the concentration of ethylene glycol in PPM and its effect on the equation , RE in equation (10) varies from (1.5×10⁴ – 2.7×10⁴),and also the maximum error is shown at every concentration.

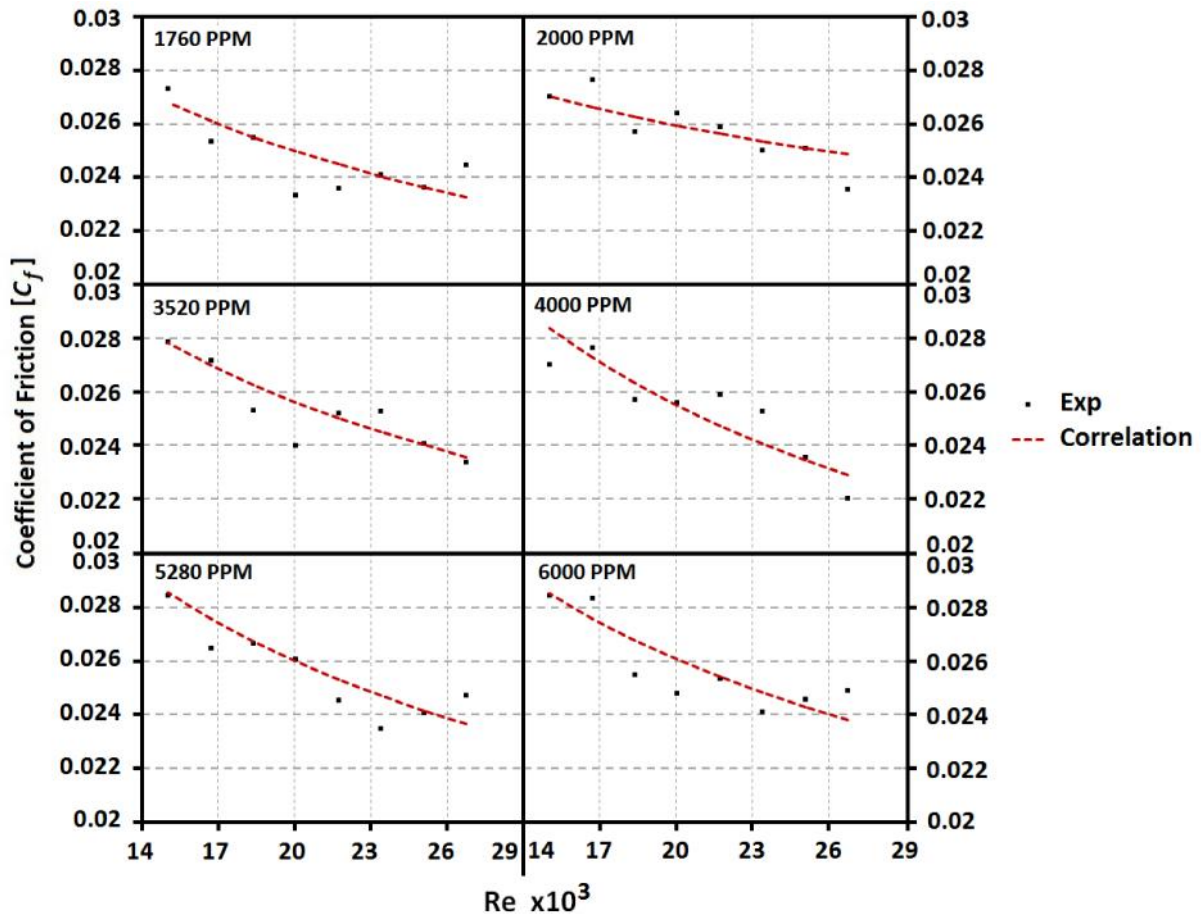


Figure 14: coefficient of friction of experimental and correlations

Figure 14 shows a comparison between experimental and correlations results regarding the coefficient of friction at different Reynolds numbers. The maximum error in all correlations was less than 0.2% which indicates the reliability of these correlations.

5- Conclusions

Within the range of the present study, the following concluding remarks are based on the numerical results, which showed fair agreement with the experimental results regarding the percentage drag reduction, obtained for adding ethylene glycol to the piping system at different concentrations and Reynolds numbers. First of all ethylene glycol could be used not only as an antifreeze but also as a drag reducing agent in district cooling systems, so behind its original benefits, now there is a new benefit of using it that it will reduce the consumed power to pump water. The results show that ethylene glycol has small drag reduction effect at concentrations up to 1000 PPM. The maximum percentage drag reduction for ethylene glycol occurs approximately at concentration of 4000 PPM. An empirical correlation between Reynolds number and concentration has been developed to estimate the DR%. These correlations showed a good agreement with the experimental results with a maximum error ranging from 0.1% to 0.16%.

Nomenclature:

Symbol	Description	Unit
C_f	Coefficient of friction	--
ρ	Specific density	kg/m ³
μ	Dynamic viscosity	kg/m.s
ν	Kinematic viscosity	m ² /s
V	Velocity	m/s

D	Diameter	m
VBI	Viscosity Blending Index of the blend	--
C_{fp}	Friction factor for mixture	--
C_{fw}	Friction factor for water	--
Re	Reynolds number	--
H	Head	m
$F_{blasius}$	theoretical friction factor	--
$F_{measured}$	actual friction factor	--
L	Length	m
Q	Flow rate	m^3/s
K	Turbulence kinetic energy	m^2/s^2
	Turbulence dissipation rate	m^2/s^3
G	Gravity	m/s^2
PPM	Parts per millions	--
T_i	Turbulence intensity	%
DR	Drag reduction percentage	%

References

- [1]. Hartman company (2005)
- [2]. Yeshayahu Talmon, David J. Hart "Development of Practical Drag Reduction System for District Cooling Systems " Ohio university ,2005
- [3]. Toms, B.A., (1949), "Some observations on the flow of linear polymer solutions through straight tubes at large Reynolds numbers", Proc. Int. Cong. on Rheology, Vol. II, pp.135-141.
- [4]. Yoon, S.M., Kim, N.J., Kim, C.B., Hur, B.K., (2002) "Flow and heat transfer characteristics of drag reduction additives in district heating and cooling systems" J. Ind. Eng. Chem., Vol. 8, No. 6, pp. 564-571,.
- [5]. Kawaguchi et al. (2007), "Use of friction reducing additives in district heating system".
- [6]. Lumley, J.L., (1969), "Drag reduction by additives", Ann. Rev. Fluid Mech. 1, pp. 367–384.
- [7]. Lumley, J.L., (1973), "Drag reduction in turbulent flow by polymer additives", J. Polym. Sci. Macromol. Rev. 7, pp. 283–290.
- [8]. Selim, M.M., (2011), "Energy saving in Irrigation Piping Systems using Fertilizer", M.Sc. thesis, Arab Academy for Science, Technology, and Maritime Transport.
- [9]. Rodi, W. and Mansour, N.N., (1993), "Low Reynolds Number k-epsilon Modeling with the Aid of Direct Simulation Data", J. of Fluid Mechanics, Vol. 250, pp. 509-529.
- [10]. Patel, V.C., Rodi, W. and Scheuerer, G., (1985), "Turbulence Models for Near-Wall and Low Reynolds Number Flows: A Review", AIAA J., Vol. 23, pp. 1308-1319.
- [11]. Warda, H.A., Kassab, S.Z., Shawky, M.A., and Abdallah, S.A., (1990), "Experimental Study of The Effectiveness of Some Coagulant Aids as Drag Reducing Agents," Alexandria Engineering J., Vol. 29, pp. 279-284.
- [12]. Gampert B. and Rensch A. , (1996), "Polymer concentration and near-wall turbulence structure of channel flow of polymer solutions", ASME FED-237, J. Fluids Eng. Div. Conf., No. 2, pp. 129-136.
- [13]. Allahdadi, M.M. and Sadeghy, K., (2008), "Simulating drag reduction phenomenon in turbulent pipe flows", Mechanics Research Communications, Vol. 35, pp. 609–613.
- [14]. Lemenand, T., Dupont, P., Della Valle, D., (2005), "Turbulent Mixing of Two Immiscible Fluids," J. Fluids Eng., Transactions of the ASME, 127(6) pp. 1132-1139.
- [15] versteeg H.K., Malalsekera, H.w.,(1995), "Introduction to computational fluid dynamics: The finite volume method".(Harlow, Essex, England and Longman scientific and technical), Newyork, USA.